中国光学（中英文） Chinese Optics 核心期刊

基于光纤U形腔的马赫–曾德尔干涉仪的磁场传感器

范鹏程 蒋学赛 田德强 张光强

Magnetic field sensor utilizing U-Shaped Cavity based on in-fiber Mach–Zehnder interferometer

FAN Peng-cheng, JIANG Xue-zhai, Tian De-qiang, Zhang Guang-qiang

引用本文:
范鹏程, 蒋学赛, 田德强, 张光强. 基于光纤U形腔的马赫–曾德尔干涉仪的磁场传感器[J]. 中国光学, 2024, 17(3): 674–682. doi: 10.37188/CO.EN–2023–0015
FAN Peng-cheng, JIANG Xue-zhai, Tian De-qiang, Zhang Guang-qiang. Magnetic field sensor utilizing U-Shaped Cavity based on in-fiber Mach–Zehnder interferometer[J]. *Chinese Optics*, 2024, 17(3): 674-682. doi: 10.37188/CO.EN-2023-0015

在线阅读 View online: https://doi.org/10.37188/CO.EN–2023–0015

文章编号 2097-1842(2024)03-0674-09

Magnetic field sensor utilizing U-Shaped Cavity based on in-fiber Mach–Zehnder interferometer

FAN Peng-cheng*, JIANG Xue-zhai, Tian De-qiang, Zhang Guang-qiang
(*Crrc Zhuzhou Institute Co., Ltd., Zhuzhou* 421000, *China*)
* *Corresponding author*, *E-mail*: *fpc*19920528@126.*com, fanpc@csrzic.com*

Abstract: An optical fiber magnetic field sensor is proposed and experimentally demonstrated by using a U-shaped cavity based on in-fiber Mach-Zehnder interferometer (MZI) coated with magnetic fluid (MF). The magnetic field sensor is manufactured by splicing a section of single-mode fiber (SMF) between two sections of SMF with designed fiber geometric relationships. As the geometric symmetry MZI is strongly sensitive to the surrounding refractive index (RI) with a high sensitivity up to −13 588 nm/RIU and MF's RI is sensitive to magnetic field, the magnetic field sensing function of the proposed structure is realized. The results show that the magnetic field sensitivity reaches as high as 137 pm/Oe, and the magnetic field range is almost linear from 0 to 250 Oe. The proposed magnetic field sensor has the advantages of small size, low cost, easy to manufacture, robustness, high sensitivity, good repeatability and easy to integrate with fiber optic systems.

Key words: magnetic field sensor; magnetic fluid; U-shaped cavity; optical sensor

基于光纤 U 形腔的马赫-曾德尔干涉仪的磁场传感器

范鹏程*, 蒋学寨, 田德强, 张光强
（中车株洲电力机车研究所有限公司 株洲 421000）

摘要: 本文研制了一种光纤磁场传感器, 使用涂有磁流体(MF)的全光纤马赫-曾德尔干涉仪(MZI)的 U 形腔体进行实验验证。光纤磁场传感器是在两段单模光纤(SMF)之间拼接一段单模光纤形成 U 型光学腔制造而成的, 该设计具有光纤几何关系。由于几何对称性 MZI 对周围折射率(RI)具有很强的敏感性, 灵敏度高达−13 588 nm/RIU, 且磁流体的折射率对磁场敏感, 因此所提结构实现了磁场传感功能。实验结果表明, 该传感器磁场灵敏度高达 137 pm/Oe, 磁场范围从 0 ~ 250 Oe 几乎呈线性。本文所设计的光纤磁场传感器具有体积小、成本低、易于制造、坚固耐用、灵敏度高、重复性好、易于与光纤系统集成等相关优势。

关 键 词: 磁场传感器; 磁流体; U 型腔体; 光纤传感器
中图分类号: TN253 **文献标志码:** A **doi:** 10.37188/CO.EN-2023-0015

收稿日期: 2023-07-06; **修订日期:** 2023-08-07
基金项目: 中车株洲电力机车研究所有限公司资助
Supported by the Crrc Zhuzhou Institute Co., Ltd.

1 Introdution

Optical fiber magnetic field sensors have been extensively studied for both scientific and industrial applications[1-3]. Compared to other traditional magnetic field sensors, optical fiber magnetic field sensors are known for good resistance to electromagnetic interference, light weight, good safety, high sensitivity, and easy integration into optical fiber systems. Therefore, scientific and industrial applications of optical fiber magnetic field sensors have been deeply studied. Many different optical fiber magnetic sensors have been researched by combining magnetic fluid with an optical fiber device, such as long-period fiber grating[3], Sagnac interferometer structure[4], microfiber knot resonator[5], microfiber taper[6-8], microstructured optical fiber long-period grating[9], and fluid-filled photonic crystal fibers[10]. However, these sensors' sensitivity[3-5] can only reach tens pm/Oe order of magnitude and only in a narrow magnetic field strength range. Although these sensors' sensitivity[6-10] increased, they have all kinds of faults and could not be widely used because of their complex construction and vulnerabilities; at the same time, fiber Mach-Zehnder interferometers have been developed extensively for some decades[8, 11-13]. In recent years, there have been a number of research papers on the use of fiber optic MZIs and magnetic fluids to measure magnetic fields[14-17]; however, this paper proposes a novel structure in which the fiber MZIs with double optical interference arms are featured for their flexible structure, simple manufacturing process, ease of manipulation, and high sensitivity. Among different fiber MZI configurations, the in-line fiber MZI that integrates the two interference arms into a single fiber is more attractive for its in-line and convenient operation mode that requires neither a delay line nor additional fiber alignment[16-18]. Zhang's[18] research has been published as a summary article on the theme of fiber optic magnetic field sensors, introducing the basic principles, development trends, and application status of fiber optic magnetic field sensors. But, we proposed a novel in-line fiber MZI configuration for magnetic field detection.

In this paper, we proposed an easy way to detect magnetic field strength. We manufactured a magnetic field sensor based on an in-fiber MZI by combination of the U-shaped cavity, MF, and organic glass capillary. This structure's large proportion of evanescent field energy is due to part of the light beam being propagated in the solution and the other in the cladding of fiber. It has a refractive index sensitivity of up to −13 588 nm/RIU (1.33−1.36). This kind of material has many magneto-optical properties, such as the Faraday effect, RI tenability, optical scattering changeability, and thermal lens effect[19-25]. By placing the U-shaped cavity into an MF, we can get a compactly structured optical magnetic field sensor, using the in-fiber MZI to detect the interference wave, with the increase of magnetic field intensity, one of the physical lengths of our interferometer arms will change. It contains much information about magnetic field. By using an optical spectrum analyzer, we can closely follow the relationship between spectral dips and the external magnetic field.

2 Sensing configuration and principle

Figure 1(b) shows our experimental setup to measure the magnetic field and refractive index sensor based on Mach-Zehnder interferometer structure. The manufacturing process of this device is as follows: A section of standard single-mode fiber-28 with core and cladding diameters of 8.2 μm and 125 μm and length of 345 μm is spliced with two segments of SMFs with dislocation splicing of 62.5 μm. During the splicing process, a section of fiber is stepped approaching the SMF by using a fiber splicer (Fujikura FSM-100P+, in manual oper-

ation mode) with fiber cladding calibration along half of the other fiber core as shown in Figure 1(a). After splicing the first joint, we cleaved the weld misalignment of optical fiber with designed length with the assistance of a precision cleaver. Then, we put the fiber tip in the splicer at its original position and calibrated the second SMF tip in the opposite way (similarly to the first step); the second joint is controlled to make sure that the misalignment of optical fiber and the output SMF process has the same relative offset situation as its input counterpart. The discharge electric's intensity ought to be extraordinary weak and of short duration . The sensor is manufactured simply by fusion splicing and then sealed into a capillary tube filled with magnetic fluid, namely the fiber-assisted U-shaped cavity. The U-shaped cavity arm carrying samples is constructed by a section of SMF between two sections of SMF with predesigned lateral offset of the fiber. The structure is very compact and stable.

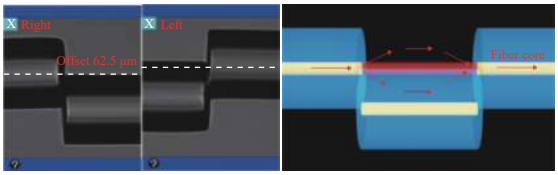

Fig. 1 (a) Side view micrograph of the left and right splicing points of the in-line MZI; (b) confronted view micrograph of the MZI in air

Figure 1(b) shows a schematic diagram of our designed MZI sensor. From this diagram, we can see that when light is launched through the first splicing point on the left, the beam will separate into two portions, with one propagating through the air in the cavity (taking light pathI_1) and the other propagating through the assistant fiber of the cladding (pathI_2). At the second splicing point, the two beams will combine and interfere with each other. The interference intensity is expressed by (1):

$$I = I_1 + I_2 + 2\sqrt{I_1 I_2}\cos\theta \quad , \qquad (1)$$

where I_1 and I_2 are the intensities along the two light paths and $\theta\left(\theta = 2\pi\Delta n_{\text{eff}}\frac{L}{\lambda} + \theta_0\right)$ is the phase difference; $n_{\text{eff}}(\approx 0.445)$ is the difference between the effective refractive index of the fiber cladding and that of the cavity in the solution; λ is the wavelength; L is the trench length; and θ_0 is the initial interference phase. When the phase difference $\theta = (2m+1)\pi$, m=0, 1, 2…, the transmission minima occurs at: $\lambda_m = 2L\Delta n_{\text{eff}}/2m+1$, where λ_m refers to the central wavelength of the mth order interference dip. The spectral fringe spacing between adjacent interference notches (free spectral range (FSR)) could be approximately calculated by equation (2), so shows that the FSR decreases as the n_{eff} increases when cavity L is fixed.

$$\text{FSR} \approx \lambda^2/\Delta n_{\text{eff}} L \quad , \qquad (2)$$

when an external perturbation (such as a change in magnetic field strength or the external RI) is imposed upon the sensing section, the RI of the MF will change. Therefore, the effective RI difference will also change, resulting in a shift of the interference valley. The light launching into the device separates along the two interference arms: the cavity (I_1) and the fiber cladding (I_2). Assuming that the Rl of one interference arm of U-shaped cavity sensor is n_{cav}, which varies with the change in the refraction of the magnetic fluid, and the effective Rl of the other physical arm which is the fiber cladding, is n_{cla}, the wavelength shift of the transmission dip, which represents the sensitivity of the sensor, can be given by $\Delta\lambda_m = 2L(n_{\text{cav}} - n_{\text{cla}})/(2m+1)$. Assuming the cavity length is a constant in our experiments, the RI sensitivity (S_{RI}) derived from Eq. (3) can be described as:

$$S_{\text{RI}} = \frac{\mathrm{d}\lambda}{\mathrm{d}(n_{\text{cav}}, n_{\text{cla}})} = \frac{\Delta\lambda_m}{\Delta n_{\text{eff}}} \quad , \qquad (3)$$

where the Δn_{eff} is equal to the difference of the effective RI of the cavity and the effective RI of the fiber cladding mode. Eq. (3) shows that the greater the variation of effective RI difference, the higher the sensitivity. So, the type of MF will have a great impact on the sensor's sensitivity.

3　Experimental results and analysis

Preliminary results of using the sensor to measure the refractive index of sucrose/water solutions were successfully demonstrated. The variable RI liquid was prepared by using deionized water dissolved with sucrose that form a high concentration of saturated sucrose solution. Figure 2 (color online) shows the interference spectrum of the fabricated sensor in air and water when a supercontinuum broadband light source and an optical spectrum analyzer are used to record the transmission spectrum change.

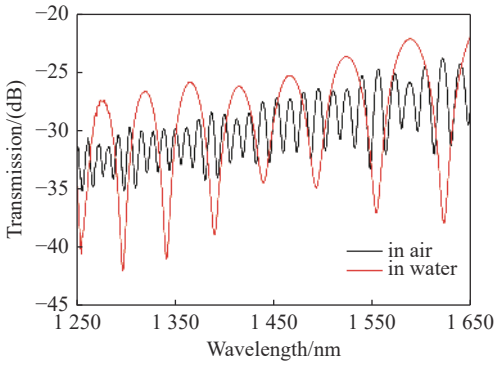

Fig. 2　Transmission spectra of the interference in air and water

Its interference spectrum shows a fringe visibility of about 5 dB in air, which is sufficient for most wavelength-interrogated sensing applications. We also know the free spectral range broadened, and the extinction ratio increased in water. This all results from the Mach–Zehnder interferometer structure. The signal intensity and fringe visibility vary with the change of liquid RI sample in the U-shaped cavity because the transmission loss and the ratio of light path I_1 to I_2 depend on the ambient RI. The transmission loss is higher in air than in water, so when two beams of light form the interference by coupling at the second splicing point, the extinction ratio is higher than in the air. Certainly, according to Eq. (2), when fixed the cavity L=345 μm, the FSR increases as the Δn_{eff} decreases, and the effective RI in air is greater than in water (Δn_{eff}=0.12 in water greater than Δn_{eff}=0.442 in air). In wavelengths around 1 550 nm, the FSR is approximately 58 nm in water and 15.7 nm in air. This illustrates that the experiment is consistent with theoretical research. To evaluate the RI measurement capability of this sensor, it has been tested using water and high concentrations of saturated sucrose solution as RI samples.

To compare the RI-dependent spectral characteristics, the transmission spectra of the RI sensor when immersed in different RI liquids are also shown in Figure 3(a) (color online). The signal intensity and fringe visibility vary with the change of liquid RI sample. With the increase of the RI, the dip wavelength smoothly blueshifts. The dependence of dip wavelength blueshifts on external RI can be expressed by Eq. (3). Since the n_{cav} is lower than the n_{cla}, the two values subtraction is negative. So, the whole formula is negative. With the increment of n_{cav}, λ_m smoothly blueshifts. The RI sensitivity sharply rises when n_{cav} is close to n_{cla}. Without a doubt, when n_{cav} is higher than n_{cla} and thus the interference dips, there is a shift toward the longer wavelength region. Figure 3(b) shows the measured transmission dip (a) applied against the different RIs. It decreases linearly from 1 622 nm to 1 270 nm when the RI changes from 1.33 to 1.34. The sensitivity is −13 588 nm/RIU in this range (1.33−1.36). And then in high RI the sensitivity is higher. According to the S_{RI} in Eq. (3), assuming a wavelength of 1 620 nm, Δn_{eff}≈0.12 (part of the light propagating in the water (n=1.322), the other in the fiber cladding (n=1.442), taking dispersion of light into consideration), then the S_{RI} is −13 431 nm/RIU. The experimental results accord strongly with the calculated results of Eq. (3). Certainly, sensing experiments have been carried out to test the response to temperature. The U-shaped cavity is placed inside a temperature-controlled chamber with a temperature range from 20 °C to 95 °C in steps of 5 °C. As temperature increases, the wavelength redshifts. In wavelengths of around 1 550 nm, the temperature sensitivity is only 29 pm/°C. Because of the small

thermal expansion of the silicon dioxide material, both the mode field distribution and the effective RI of the core mode and each cladding mode vary only a little with the temperature's variation.

Based on previous studies of RI, we have found that the sensor is very sensitive to the RI. Moreover, the RI of magnetic fluid can be tuned by magnetic field[26]. So, we can make a compact magnetic field sensor based on our designed structure. Figure 4 illustrates the experimental setup of the magnetic field sensing measurement. The sensing structure is placed between two electromagnets to generate the magnetic field and a tunable voltage source (TVS) to tune the intensity of the external magnetic field. The strength of the magnetic field is adjusted by tuning the magnitude of the supply current. The direction of the magnetic field is parallel to the optical fiber axis. In order to measure the magnetic field intensity, a gauss meter (GM) with a resolution of 0.1 Oe is placed perpendicularly to the external magnetic field. The MF used in this experiment is EMG 705. The nanoparticles in the MF are dispersed homogeneously without magnetic fields, and the RI changes with the external magnetic field. Before use, it needs to be diluted with deionized water in proportions of 9.5:0.5. When no magnetic field is applied, RI of MF EMG 705 is estimated to be around 1.34. The fabricated structure was inserted into a capillary tube with a length and inner diameter of 2 cm and 300 μm, respectively. After the capillary tube was filled with MF by capillary force, the two ends of the capillary tube were immediately sealed with UV glue.

The transmission spectra of the magnetic field sensor under different magnetic field intensities are presented in Figure 5(a) (color online). A distinct decrease in transmission can be observed in the spectrum. This is attributed to fractional mode power extending outside of the U-shaped cavity and to the absorptive properties of MF. As the magnetic field intensity increases from 0 Oe to 320 Oe at a temperature of 25 °C, the transmission loss simultaneously increases. The measured result can be explained by the tunable RI of the MF. In other words, the RI of the MF will increase with the increase of the applied magnetic field intensity[26-27]. Meanwhile, Figure 5(b) (color online) shows the variation of the effective RI of the MF. Due to the absence of a magnetic field, the nanoparticles of the magnetic fluid are not affected by magnetic force, so their positions in the U-shaped cavity of the optical fiber are random. This state provides a uniform starting point for subsequent magnetic field applications, so that when a magnetic field is applied, the nanoparticles of the magnetic fluid will be arranged in a regular manner under the action of the magnetic field, thereby affecting their refractive index of the magnetic fluid. The change in refractive index can cause changes in the interference waveform of optical fibers. The transmission spectrum has a significant blueshift until the magnetic field intensity increases to a saturated value of 260 Oe. The nonlinear response behavior of the magnetic field sensor based on in-fiber MZI is inevitable because of the saturation magnetization effect of MF. We found four sensitive and linear regions according to the peak shift for different applied magnetic field intensities. From the picture, we can know that when the magnetic field increases to 260 Oe, loss peaks will no longer move because of the saturated magnetization of the MF. On the basis of the blueshift of the four loss peaks with the magnetic field intensity increased (the change in magnetic field means an increase in environmental RI, similar to the previous measurement of the RI in sucrose water), we achieved resolution of magnetic field sensing of about 159 pm/Oe (R^2=0.994 5) in interference loss peak *d*, 148 pm/Oe (R^2=0.985) in loss peaks *c*, 140 pm/Oe (R^2=0.994) in loss peaks *b*, 137 pm/Oe (R^2=0.995) in loss peaks *a* with magnetic field intensity range from 0 to 250 Oe, as shown in Figure 5(d). When monitoring different dip wavelengths, Figure 5(d) demonstrates that the wavelength and the magnetic field are sensitive. Finally, we would like to point out a minimum magnetic field sensitivity that has the highest linear correlation with loss

peak *a*. Magnetic field intensity ranges from 0 to 250 Oe and wavelength blueshift ranges from 1 394 nm to 1 361 nm. Figure 5(c) shows the average sensitivity as 137 pm/Oe. From Figure 5(a)−5(b) we can see that our fiber optic magnetic field sensor has high repeatability. The intensity of the transmission dip change results primarily from the intensity ratio variation between the two modes (with one part of the beam of light propagated in the MF, and the other propagated in the fiber cladding). Increasing magnetic field strength, which indicates the scattering and absorption effects of MF, helped to balance the two modes' intensity. Also because of the saturation magnetization of MF, there is a saturated point of magnetic field strength at around 260 Oe, beyond which the transmission dip intensity hardly changes. The two saturation magnetic field strengths are slightly different. That may be caused by the deviation of RI change and nanoparticle agglomeration process in the MF. However, it does not influence our measurement of magnetic field in the linear response range. We can easily see the performance parameters of fiber optic magnetic field sensors in Table 1 of Reference [18]. The magnetic field sensitivity of the optical fiber magnetic field sensor we designed is much higher than that of FBG, LPFG, TFBG and other sensing structures. The temperature effect on the performances of the magnetic field sensor has also been experimentally investigated. At different temperature increments, we find the wavelength dip shift obviously. The wavelength around 1 500 nm red shifted to 1 650 nm. The temperature sensitivity is upping to 3.08 nm/°C at range of 25 °C from 95 °C. The high temperature response is caused by high S_{RI} of the in-fiber MZI. The simultaneous measurement of magnetic field and temperature has been proven in our previous research[28] and Gu's research[29]. Ref. [28] can guide us to overcome the influence of temperature on magnetic fields. Therefore, it will not be described in this article deeply. Optical fiber magnetic field sensors and magnetically sensitive materials involved in these sensors have some common problems. The industrialization of these optical fber sensors needs to be improved. The problems of device packaging and the improvement of stability still need to be solved. These are the engineering requirements that continue to drive our research. There are many methods for measuring magnetic field strength using optical fibers, each with its own advantages and disadvantages. The focus of this article is on the manufacturability and stability of the sensor. In practical applications, only quasi distributed measurements are currently possible[18]. We will also continue to strive in the direction of quasi distribution measurement.

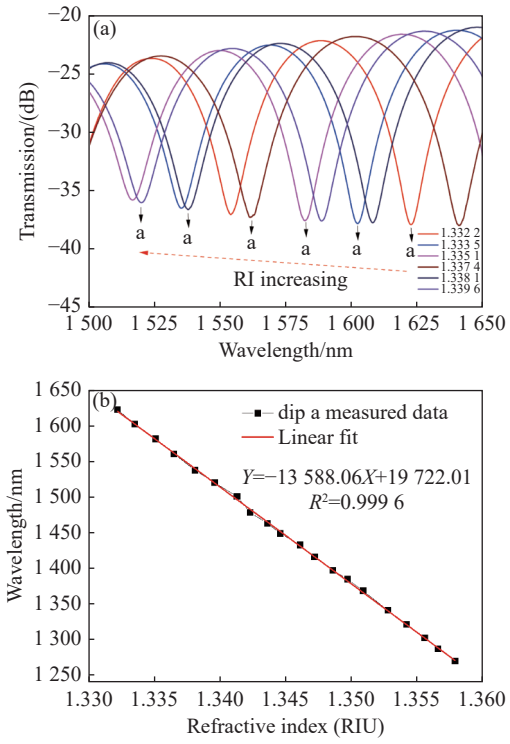

Fig. 3　(a) Interference spectra at different RI values and (b) spectral RI response of the proposed RI sensor

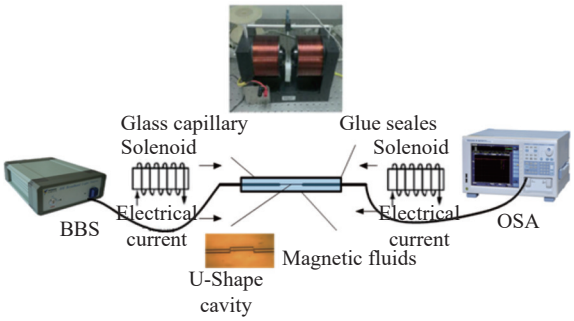

Fig. 4　Schematic diagram of the magnetic field sensor. Inset is the cross-sectional view of the U-shaped cavity, combined with an MF sealed into a capillary

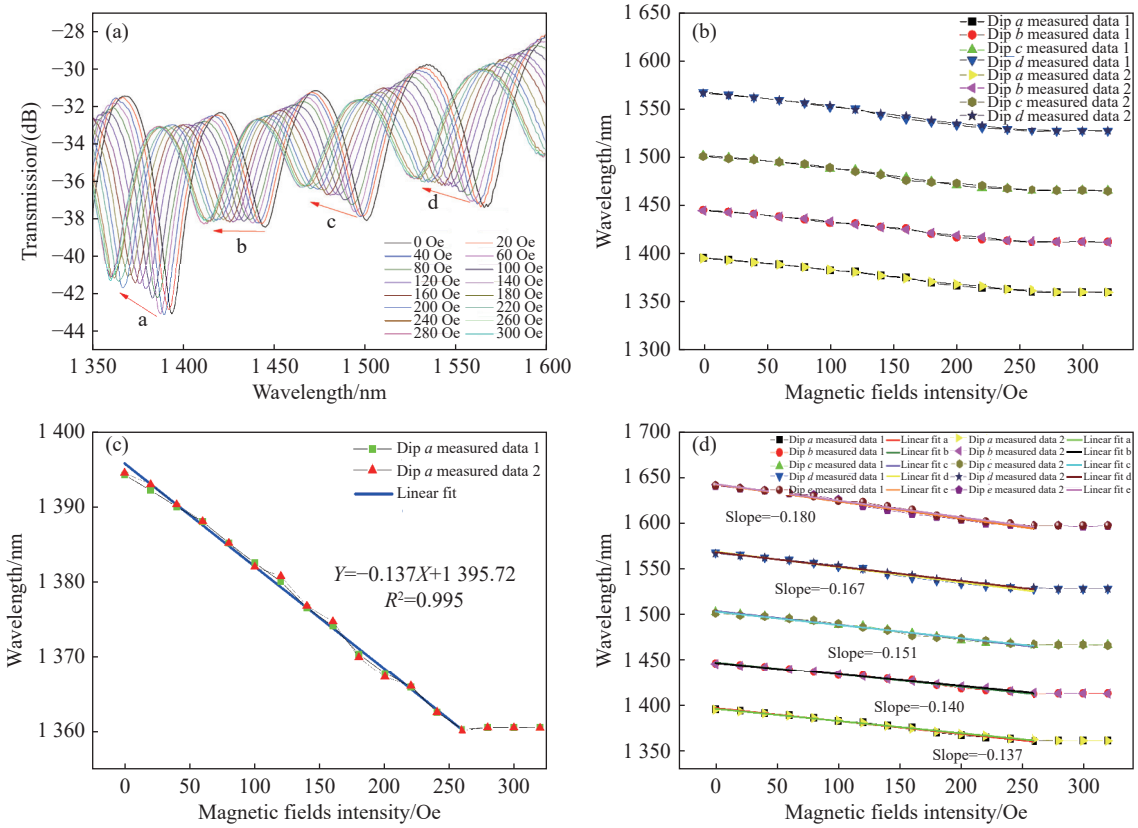

Fig. 5 (a) Variation of a dip spectrum with the applied magnetic field. (b) Loss peak *a*, *b*, *c*, *d* wavelength as a function of the magnetic field strength. (c) (d) Loss peak *a* wavelength shift as a function of magnetic field strength

4 Conclusion

A magnetic fluid-based magnetic field sensor is realized and experimentally demonstrated by using an in-fiber Mach–Zehnder interferometer. This structure has the advantages of stability, compactness, and a large proportion of evanescent field energy, because of part of the energy moving through the air, the other through the cladding of fiber. So the RI of the MF changes as the magnetic field strength, and the transmission spectrum of the in-fiber MZI is thereby modulated. Because of the U-shaped cavity based on the in-fiber MZI being very sensitive to RI (−13 588 nm/RIU), we can detect the magnetic field strength by monitoring the wavelength shift. Within a magnetic field range from 0 to 250 Oe, the wavelength shift varying with the magnetic field has a good linear relationship, but also the sensitivity achieved is up to 137 pm/Oe. Our sensor possesses low cost, repeatability, fiber-compatibility and high sensitivity.

References:

[1] HORNG H E, CHIEH J J, CHAO Y H, *et al*.. Designing optical-fiber modulators by using magnetic fluids[J]. *Optics Letters*, 2005, 30(5): 543-545.

[2] PU SH L, CHEN X F, CHEN Y P, *et al*.. Measurement of the refractive index of a magnetic fluid by the retroreflection on the fiber-optic end face[J]. *Applied Physics Letters*, 2005, 86(17): 171904.

[3] LIU T, CHEN X F, DI Z Y, *et al*.. Tunable magneto-optical wavelength filter of long-period fiber grating with magnetic fluids[J]. *Applied Physics Letters*, 2007, 91(12): 121116.

[4] ZU P, CHAN C C, LEW W S, *et al*.. Magneto-optical fiber sensor based on magnetic fluid[J]. *Optics Letters*, 2012, 37(3): 398-400.

[5] LI X L, DING H. All-fiber magnetic-field sensor based on microfiber knot resonator and magnetic fluid[J]. *Optics Letters*, 2012, 37(24): 5187-5189.

[6] MIAO Y P, WU J X, LIN W, *et al*.. Magnetic field tunability of optical microfiber taper integrated with ferrofluid[J]. *Optics Express*, 2013, 21(24): 29914-29920.

[7] LAYEGHI A, LATIFI H, FRAZAO O. Magnetic field sensor based on nonadiabatic tapered optical fiber with magnetic fluid[J]. *IEEE Photonics Technology Letters*, 2014, 26(19): 1904-1907.

[8] ZHENG Y Z, DONG X Y, CHAN C C, *et al*.. Optical fiber magnetic field sensor based on magnetic fluid and microfiber mode interferometer[J]. *Optics Communications*, 2015, 336: 5-8.

[9] MIAO Y P, ZHANG K L, LIU B, *et al*.. Ferrofluid-infiltrated microstructured optical fiber long-period grating[J]. *IEEE Photonics Technology Letters*, 2013, 25(3): 306-309.

[10] GAO R, JIANG Y, ABDELAZIZ S. All-fiber magnetic field sensors based on magnetic fluid-filled photonic crystal fibers[J]. *Optics Letters*, 2013, 38(9): 1539-1541.

[11] WO J H, WANG G H, CUI Y, *et al*.. Refractive index sensor using microfiber-based Mach–Zehnder interferometer[J]. *Optics Letters*, 2012, 37(1): 67-69.

[12] TIAN Z B, YAM S S H, BARNES J, *et al*.. Refractive index sensing with Mach–Zehnder interferometer based on concatenating two single-mode fiber tapers[J]. *IEEE Photonics Technology Letters*, 2008, 20(8): 626-628.

[13] XUE Y, YU Y S, YANG R, *et al*.. Ultrasensitive temperature sensor based on an isopropanol-sealed optical microfiber taper[J]. *Optics Letters*, 2013, 38(8): 1209-1211.

[14] LUO Y, LEI X Q, SHI F Q, *et al*.. A novel optical fiber magnetic field sensor based on Mach-Zehnder interferometer integrated with magnetic fluid[J]. *Optik*, 2018, 174: 252-258.

[15] LEI X Q, XU Y CH, YU Y T, *et al*.. Fiber in-line magnetic field sensor based on Mach-Zehnder interferometer integrated with magnetic fluid[J]. *Optoelectronics Letters*, 2019, 15(1): 43-47.

[16] LI ZH Y, LIAO CH R, SONG J, *et al*.. Ultrasensitive magnetic field sensor based on an in-fiber Mach–Zehnder interferometer with a magnetic fluid component[J]. *Photonics Research*, 2016, 4(5): 197-201.

[17] CAI SH H, SERGEEV M, PETROV A, *et al*.. Highly sensitive vector magnetic field sensors based on fiber Mach–Zehnder interferometers[J]. *Optics Communications*, 2022, 524: 128725.

[18] ZHANG J, WANG CH, CHEN Y K, *et al*.. Fiber structures and material science in optical fiber magnetic field sensors[J]. *Frontiers of Optoelectronics*, 2022, 15(1): 34.

[19] GAO SH CH, ZHANG W G, GENG P CH, *et al*.. Highly sensitive in-fiber refractive index sensor based on down-bitaper seeded up-bitaper pair[J]. *IEEE Photonics Technology Letters*, 2012, 24(20): 1878-1881.

[20] GAO SH CH, ZHANG W G, ZHANG H, *et al*.. Reconfigurable and ultra-sensitive in-line Mach-Zehnder interferometer based on the fusion of microfiber and microfluid[J]. *Applied Physics Letters*, 2015, 106(8): 084103.

[21] KONSTANTAKI M, CANDIANI A, PISSADAKIS S. Optical fibre long period grating spectral actuators utilizing ferrofluids as outcladding overlayers[J]. *Journal of the European Optical Society - Rapid Publications*, 2011, 6: 11007.

[22] DAI J X, YANG M H, LI X B, *et al*.. Magnetic field sensor based on magnetic fluid clad etched fiber Bragg grating[J]. *Optical Fiber Technology*, 2011, 17(3): 210-213.

[23] DONG SH H, PU SH L, HUANG J. Magnetic field sensing based on magneto-volume variation of magnetic fluids investigated by air-gap Fabry-Pérot fiber interferometers[J]. *Applied Physics Letters*, 2013, 103(11): 111907.

[24] ZU P, CHAN C C, LEW W S, *et al*.. Temperature-insensitive magnetic field sensor based on nanoparticle magnetic fluid and photonic crystal fiber[J]. *IEEE Photonics Journal*, 2012, 4(2): 491-498.

[25] DENG M, SUN X K, HAN M, *et al*.. Compact magnetic-field sensor based on optical microfiber Michelson interferometer and Fe_3O_4 nanofluid[J]. *Applied Optics*, 2013, 52(4): 734-741.

[26] YANG S Y, CHIEH J J, HORNG H E, *et al*.. Origin and applications of magnetically tunable refractive index of magnetic fluid films[J]. *Applied Physics Letters*, 2004, 84(25): 5204-5206.

[27] LUO L F, PU SH L, TANG J L, *et al*.. Reflective all-fiber magnetic field sensor based on microfiber and magnetic fluid[J]. *Optics Express*, 2015, 23(14): 18133-18142.

[28] LI J, FAN P CH, TIAN ZH, *et al*.. Potential for simultaneous measurement of magnetic field and temperature utilizing fiber taper modal interferometer and magnetic fluid[J]. *IEEE Photonics Journal*, 2016, 8(6): 6805609.

[29] GU SH F, SUN W, LI M, *et al*.. Simultaneous measurement of magnetic field and temperature based on photonic crystal

fiber plasmonic sensor with dual-polarized modes[J]. *Optik*, 2022, 259: 169030.

Author Biographics:

FAN Peng-cheng (1992—), male, born in Hengyang, Hunan, Master degree, obtained his bachelor degree and master degree in Hunan University of Science and Engineering and Jinan University in 2014 and 2017, respectively.The main research directions are fiber optic sensing technology, LCD display, OLED display, and human-computer interaction technology. E-mail: fpc19920528@126.com or fanpc@crszic.com